

1 **Multiple pathways for the formation of secondary organic aerosol in North China Plain**
2 **in summer**

3 Yifang Gu^{1,4}, Ru-Jin Huang^{1,2,3,4}, Jing Duan¹, Wei Xu¹, Chunshui Lin¹, Haobin Zhong^{1,4}, Ying
4 Wang¹, Haiyan Ni¹, Quan Liu⁵, Ruiguang Xu^{6,7}, Litao Wang^{6,7}, Yong Jie Li⁸

5 ¹SKLLQG, Center for Excellence in Quaternary Science and Global Change, Institute of Earth
6 Environment, Chinese Academy of Sciences, Xi'an 710061, China

7 ²Open Studio for Oceanic-Continental Climate and Environment Changes, Pilot National
8 Laboratory for Marine Science and Technology (Qingdao), Qingdao 266000, China

9 ³Institute of Global Environmental Change, Xi'an Jiaotong University, Xi'an 710049, China

10 ⁴University of Chinese Academy of Sciences, Beijing 100049, China

11 ⁵State Key Laboratory of Severe Weather & Key Laboratory of Atmospheric Chemistry of C
12 MA, Chinese Academy of Meteorological Sciences, Beijing 100081, China

13 ⁶Department of Environmental Engineering, School of Energy and Environmental Engineering,
14 Hebei University of Engineering, Handan 056038, China

15 ⁷Hebei Key Laboratory of Air Pollution Cause and Impact, Handan 056038, China

16 ⁸Department of Civil and Environmental Engineering, and Centre for Regional Oceans, Faculty
17 of Science and Technology, University of Macau, Taipa, Macau 999078, China

18 *Correspondence to:* Ru-Jin Huang (rujin.huang@ieecas.cn)

19

20

21 **Abstract**

22 Secondary organic aerosol (SOA) has been identified as a major contributor to fine
23 particulate matter (PM_{2.5}) in North China Plain (NCP). However, the chemical mechanisms
24 involved are still unclear due to incomplete understanding of its multiple formation processes.
25 Here we report field observations in summer in Handan of NCP, based on high-resolution
26 online measurements. Our results reveal the formation of SOA via photochemistry and two
27 types of aqueous-phase chemistry, the latter of which include nocturnal and daytime processing.
28 The photochemical pathway is the most important under high O_x (=O₃ + NO₂) conditions (65.1
29 ± 20.4 ppb). The efficient SOA formation from photochemistry (~~photochem-SOA~~O_x-initiated-
30 SOA) dominated the daytime (65% to OA) with an average growth rate of 0.8 μg m⁻³ h⁻¹.
31 During the high relative humidity (RH: 83.7 ± 12.5 %) period, strong nocturnal aqueous-phase
32 SOA formation (aq-SOA) played a significant role in SOA production (45% to OA) with a
33 nighttime growth rate of 0.6 μg m⁻³ h⁻¹. Meanwhile, an equally fast growth rate of 0.6 μg m⁻³ h⁻¹
34 ¹ of ~~photochem-SOA~~O_x-initiated-SOA from daytime aqueous-phase photochemistry was also
35 observed, which contributed 39% to OA, showing that photochemistry in the aqueous phase is
36 also a non-negligible pathway in summer. The primary-related-SOA (SOA attributed to
37 primary particulate organics) and aq-SOA are related to residential coal combustion activities,
38 supported by distinct fragments from polycyclic aromatic hydrocarbons (PAHs). Moreover, the
39 conversion and rapid oxidation of primary-related-SOA to aq-SOA could be possible in the
40 aqueous phase under high-RH conditions. This work sheds light on the multiple formation
41 pathways of SOA in ambient air of complex pollution, and improves our understanding of
42 ambient SOA formation and aging in summer with high oxidation capacity.

43

44 **KEYWORDS:** secondary organic aerosol, aqueous-phase chemistry, photochemistry, multiple-
45 phase chemistry, complex air pollution

46

47 1. Introduction

48 Rapid economic growth and urbanization processes have led to severe particulate air
49 pollution in China, affecting air quality, climates and human health (Huang et al., 2014;
50 Cohen et al., 2017; An et al., 2019). Organic aerosol (OA) is a major component of aerosol
51 particles, consisting of 20-90% of fine particle mass (Jimenez et al., 2009; Zhang et al., 2011).
52 OA is either emitted directly from primary sources (referred to as primary OA, POA) such as
53 traffic, cooking, coal combustion, and biomass burning, or produced through gas-to-particle
54 conversion (referred to as secondary OA, SOA) in the atmosphere. In recent years, with the
55 implementation of control measures, the POA fraction is decreasing and SOA fraction is
56 increasing in North China Plain (NCP), indicating that SOA is becoming more critical for urban
57 air quality (Huang et al., 2019; Xu et al., 2019; Gu et al., 2020). However, our understanding
58 of the formation mechanisms and evolution processes of SOA is still limited.

59 Generally, SOA can be formed through gas-phase photochemical oxidation of volatile
60 organic compounds (VOCs) followed by nucleation or condensation of oxidation products onto
61 the preexisting particles (Donahue et al., 2006). Herndon et al., (2008) showed that oxygenated
62 organic aerosol (OOA), a surrogate of SOA, was well correlated with odd oxygen ($O_x = O_3 +$
63 nitrogen dioxide (NO_2)) during photochemical processing. SOA can also be formed in the
64 aqueous phase on wet aerosols, clouds and fogs through further chemical processes of water-
65 soluble organic compounds or organic products of gas-phase photochemistry (Ervens et al.,
66 2011, 2014). A growing number of laboratory studies and field measurements have indicated
67 that aqueous-phase processes contribute efficiently to the formation of SOA (Gilardoni et al.,
68 2016; Bikkina et al., 2017). However, how photochemistry and aqueous-phase chemistry
69 coordinate to affect the formation of SOA is still unclear, despite numerous measurements to
70 explore this question using aerosol chemical speciation monitor (ACSM) or aerosol mass
71 spectrometer (AMS) (Hu et al., 2016b; Hu et al., 2017; Sun et al., 2016; Li et al., 2017; Sun et
72 al., 2018b; Huang et al., 2019; Gu et al. 2020; Kuang et al., 2020). Field measurements in
73 Beijing suggested that gas-phase photochemical oxidation can play a dominant role in SOA
74 formation (Sun et al., 2016; Hu et al., 2016a). Xu et al., (2017) showed that less oxidized-OOA
75 (LO-OOA) was mainly formed through photochemical oxidation, while the more oxidized-
76 OOA (MO-OOA) formation was dominantly formed by aqueous-phase chemistry in Beijing
77 for different seasons. Kuang et al. (2020) investigated the effects of gas-phase and aqueous-
78 phase photochemical processes on the formation of SOA and found that photochemical
79 aqueous-phase SOA formation dominantly contributed to daytime OOA formation in winter
80 Gucheng, located between Beijing (~100 km) and Baoding (~40 km) on the NCP. We found
81 that photochemical processing attributed mostly to MO-OOA in summertime Beijing (Gu et al.,
82 2020). Although these studies provided important insights into SOA formation processes, our
83 understanding on the photochemical and aqueous-phase formation pathways for SOA and their

84 impacts on oxidation degree are far from complete. This lack of understanding is especially so
85 under the conditions that atmospheric oxidative capacity and pollution characteristics have been
86 largely changing in China due to large reduction in direct emissions of air pollutants.

87 In this study, we investigated the photochemical versus aqueous-phase processing for SOA
88 composition and oxidation degree of OA in summertime Handan, which is a typical
89 industrialized city in the NCP region. The city is located at the intersectional area of Hebei,
90 Shanxi, Henan, and Shandong—four heavily urbanized and industrialized provinces (Fig. S1),
91 and it is therefore an ideal site to investigate the SOA formation pathways in the NCP region.
92 The multiple formation pathways, evolution of SOA composition, and oxidation degree under
93 different meteorological conditions were discussed, which sheds light on the aqueous-phase
94 chemistry and photochemical processing in SOA formation in the NCP region of China.

95 **2. Experimental methods**

96 **2.1 Sampling site**

97 Measurements were conducted from 10th August 2019 to 17th September 2019 on the campus
98 of Hebei University of Engineering (36.57 N, 114.50 E), located at the southeast edge of urban
99 Handan (Fig. S1). The site is surrounded by a school and residential areas, ~300 m north to
100 South Ring Road and ~400 m northeast to the Handan Highway (S313). The sampling site is
101 on the rooftop of a four-floor building, approximately 12 m above the ground.

102 **2.2 Instrumentation**

103 Real-time non-refractory PM_{2.5} composition was measured by a soot particle long time-of-
104 flight aerosol mass spectrometer (SP-LToF-AMS, Aerodyne Research Inc.) with a time
105 resolution of 1 min. The detailed instrument description and operation of AMS were reported
106 in Onasch et al., (2012). Compared to the conventional AMS, the LToF mass analyzer can
107 provide much better mass resolution of ~8000. During the campaign, the instrument was
108 operated in the “laser off” mode and only the standard tungsten vaporizer was applied.
109 Therefore, only non-refractory PM_{2.5} components (NR-PM_{2.5}) were measured, including
110 organics (Org), nitrate (NO₃), sulfate (SO₄), ammonium (NH₄), and chloride (Chl). Ambient
111 air was sampled and dried by a Nafion dryer (MD-700-24S, Perma Pure, Inc.) at a flow rate of
112 5 L min⁻¹, and then sub-sampled into the SP-LToF-AMS at a flow rate of ~ 0.1 L min⁻¹. An
113 aerodynamic PM_{2.5} lens was used to focus the particle into a beam, which was then impacted
114 on the heated tungsten surface (~ 600 °C) and flash-vaporized. Electron ionization with 70 eV
115 was used to ionize the vaporized gases. The ionization efficiency (IE) and the relative ionization
116 efficiency (RIE) calibrations (Jimenez et al., 2003) were conducted by using 350 nm
117 ammonium nitrate (NH₄NO₃) and ammonium sulfate ((NH₄)₂SO₄) particles.

118 Gaseous pollutants including SO₂ (9850 SO₂ analyzer, Ecotech), NO₂ (Model 42i NO-NO₂-
119 NO_x analyzer, Thermo Scientific), CO (Model 48i carbon monoxide analyzer, Thermo
120 Scientific), O₃ (Model 49i ozone analyzer, Thermo Scientific), and meteorological parameters
121 including RH and temperature were also measured during the observation period. Furthermore,
122 an aethalometer (Model AE-33, Magee Scientific) was deployed to measure the mass
123 concentration of black carbon (BC) at a time resolution of 1 min.

124 **2.3 Data Analysis**

125 The data analysis software (SQUIRREL, version 1.63I and PIKA, 1.23I) within Igor Pro 6.37
126 (WaveMetrics) was used to analyze the AMS data. The experimental RIE values of 4 (NH₄)
127 and 1.2 (SO₄) and the standard RIE values of 1.4 (Org), 1.1 (NO₃) and 1.3 (Chl) were used.
128 The composition-dependent collection efficiency (CDCE, Middlebrook et al., 2012) was used
129 to compensate for the incomplete detection caused by particle bounce on the vaporizer. An
130 improved Ambient (I-A) method was adopted for the elemental ratio analysis of high-resolution
131 (HR) OA mass spectra, such as oxygen-to-carbon (O:C), and hydrogen-to-carbon (H:C) ratios
132 (Canagaratna et al., 2015), which reflect the relative composition and oxidation degree for
133 different OA source. In our study, PMF was performed on HR mass spectra of OA for ions with
134 *m/z* values of 12-120, together with the signals from integer *m/z* values between 121 to 300 (i.e.,
135 unit mass resolution, UMR) using SoFi (version 6.3) in Igor Pro (Paatero, 1999; Canonaco et
136 al., 2013). The data and error matrices were preprocessed according to Elser et al., (2016) and
137 detailed description of PMF analysis was given elsewhere (Canonaco et al. 2013; Elser et al
138 2016). Unconstrained PMF solutions with varied factor numbers were analyzed and six factors
139 were resolved, including two primary and four secondary organic factors (Fig. 3). The six-factor
140 solution was preferred because the five-factor solution was not able to separate high signal of
141 *m/z* 44 (which represents high oxidation state) from primary organic aerosol (POA) factors,
142 while the seven-factor solution added additional OOA factors with similar profiles and noisy
143 time series for which no physical interpretation could be found. The two POA factors consisted
144 of a traffic-related factor (hydrocarbon-like OA, HOA) and a cooking-related factor (COA),
145 which had been resolved in previous summer studies in NCP (Elser et al., 2016; Hu et al., 2016b;
146 Sun et al., 2016; Huang et al., 2019). AMS source apportionment studies often report one or
147 two oxygenated organic aerosol (OOA) factors that are distinguished by the extent of
148 oxygenation and linked to volatility or oxidation degree. Owing to higher mass resolution of
149 LTOF-AMS and the inclusion of integer-mass signals for *m/z* from 121 to 300 for high-
150 molecular-weight species such as polycyclic aromatic hydrocarbons (PAHs), we herein
151 resolved four SOA factors. These four SOA factors include aq-SOA attributable to aqueous-
152 phase chemistry, ~~phochem-SOA~~ O_x-initiated-SOA attributable to photochemistry, primary-
153 related-SOA attributable to prompt oxidation of POA during emission, and fresh-SOA with a
154 lower *f*₄₄/*f*₄₃ ratio (fraction of *m/z* 44 and 43 in OA).

155 2.4 Aerosol liquid water content

156 The aerosol liquid water content (ALWC) was simulated by ISORROPIA-II model (Fountoukis
157 and Nenes, 2007; Hennigan et al., 2015) using the measurements of ambient inorganic species
158 (NO₃, SO₄, NH₄, and Chl) and meteorological parameters (temperature and RH). The
159 simulation was run in “metastable” mode where all components are assumed to be deliquescent
160 and contain no solid matter. The concentrations and speciation (if dissociated) of those
161 inorganic species in thermodynamic equilibrium was then simulated by the model and then the
162 ALWC was calculated. The inorganic cations such as Na⁺, K⁺, Ca²⁺, Mg²⁺ were not measured
163 and included in the simulation on account of that these crustal ions constituted relatively small
164 fractions of aerosol, and had relatively weak effects on ALWC accumulation (Fountoukis and
165 Nenes, 2007; Su et al., 2022). The ISORROPIA-II model does not consider the contribution
166 to ALWC from organics, since inorganic aerosols dominate the water uptake by ambient
167 particles with a contribution of approximate >80% of the total ALWC (Huang et al., 2020).

168 3. Results and discussion

169 3.1 SOA sources

170 In our study, SOA accounted for 69% (13.5 $\mu\text{g m}^{-3}$) of the total OA (19.6 $\mu\text{g m}^{-3}$),
171 representing the dominant fraction in OA in summer Handan. Among the four PMF-resolved
172 SOA sources (Fig. 1), ~~photochem-SOA~~ O_x-initiated-SOA dominated (31% to total OA), followed
173 by fresh-SOA (18%), aq-SOA (15%), and primary-related-SOA (5%). Since we focus on SOA
174 formation in this study, detailed descriptions of the HOA (12%) and COA (19%) is provided in
175 section 1.1 in the SI. The mass spectral profiles of the six OA source factors are shown in Fig.
176 1, while the time series of the SOA factors are shown in Fig. 2. In particular, a remarkable
177 continuous growth of aq-SOA concentration (from $\sim 0.3 \mu\text{g m}^{-3}$ to $25.2 \mu\text{g m}^{-3}$) and ALWC
178 (from $3.1 \mu\text{g m}^{-3}$ to $486.1 \mu\text{g m}^{-3}$) occurred on 24th-28th August (Fig. 2d). Meanwhile, the O:C
179 ratio indicative of OA oxidation state displayed a continuous increase from 0.52 to a maximum
180 of 0.93 during this time (Fig. 2e), consistent with the continuous increase in RH (reaching over
181 95%). This observation hints that during this period aqueous-phase processing might have
182 played an important role in aq-SOA formation. This role of aqueous-phase processing in SOA
183 formation is not just specific to this particular event, but also important in the whole campaign,
184 which is discussed in detail in section 3.3 later.

185 SOA factors were resolved depending on the oxidation state, which correspond to aged SOA
186 and fresh SOA respectively (Jimenez et al., 2009). One factor is attributed to aqueous-phase
187 chemistry (aq-SOA) and the other to photochemistry (~~photochem-SOA~~ O_x-initiated-SOA), while
188 fresher factor is produced by fresh-source (fresh-SOA) with a lower f_{44}/f_{43} ratio, and the other

189 considered as oxidized primary sources denoted as primary-related-SOA. Although all of the
190 SOA factors were characterized by higher m/z 44 (CO_2^+) and m/z 28 (CO^+) signal compared
191 with POA factors, their mass spectrum and temporal trends were noticeably distinguishable,
192 corresponding to different formation mechanism, which will be discussed in the following
193 section.

194 As shown in Fig. S3, the aq-SOA was identified as it increased with ALWC but decreased
195 with O_x , which might be produced/influenced by aqueous-phase chemistry and is defined as aq-
196 SOA. This indicates that aq-SOA was either formed via aqueous phase reactions or
197 absorbed/dissolved into aerosol liquid water. It exhibits the highest O:C ratios of all factors (0.7)
198 and a higher $f_{\text{CO}_2^+}$ to the total signal of 21.7%, but a low H:C ratio of 1.24 (Fig. 1). The photochem-
199 SOA O_x -initiated-SOA in our study is photochemical production SOA whose formation
200 initiated with the presence of O_x . As O_x has been shown to be a conserved tracer to during
201 photochemical processing (Xu et al., 2017), the relationship between O_x and O_x -initiated-SOA
202 can represent a metric to characterize SOA formation mechanisms associated with ozone
203 production chemistry SOA (Herndon et al., 2008). O_x -initiated-SOA presented an opposite
204 trend with significant increase as function of O_x but decreased as a function of ALWC (Fig. S3),
205 suggesting the dominant role of photochemical processing in the formation of O_x -initiated-SOA.

206 The fresh-SOA showed an increase substantially as ALWC increasing, similar to aq-SOA.
207 Whereas it also showed a slight increase trend following O_x when $\text{O}_x < 100$ ppb (Fig. S3).
208 Therefore, both aqueous-phase chemistry and photochemical processing were thought to have
209 positive impacts synchronously on the formation of fresh-SOA. In this study, the fresh-SOA
210 had the lowest atomic O:C ratio of 0.41 and the highest atomic H:C ratio of 1.41 among the
211 four SOA factors, corresponding with the $f_{\text{CO}_2^+}$ of 8.3%, these characteristics are consistent with
212 the global average O:C ratio of LO-OOA of 0.35 ± 0.14 , Ng et al., 2010), demonstrating the it
213 is more fresh SOA. Although the primary-related-SOA constituted a small fraction and showed
214 little variation during P1~P3 (3%~5%), this SOA source is also of particular interest because
215 of its distinctive fragments with high m/z values in the mass spectrum (Fig. 1d). At $m/z < 120$,
216 the primary-related-SOA had higher intensities for m/z 43 (mainly $\text{C}_2\text{H}_3\text{O}^+$) and m/z 44 (mainly
217 CO_2^+) than those in POA, indicating a typical nature of less-oxidized SOA. At $m/z > 120$, PAH-
218 derived fragments are clearly evident in the mass spectrum of the primary-related-SOA, as
219 indicated by PAH-like ions (described in SI 1.2) (Dzepina et al., 2007). Previous AMS studies
220 have observed pronounced peaks of PAH ions in POA mass spectra, such as those in coal
221 combustion organic aerosol (CCOA) and biomass burning organic aerosol (BBOA) (Hu et al.,
222 2016b; Zhao et al., 2019), but rarely in SOA. This observation implies that the factor may be
223 related to the POA originated from domestic coal combustion and here it is termed as primary-
224 related-SOA (Xu et al., 2006). Moreover, this SOA factor exhibited relatively better
225 correlations with some gaseous pollutants (Fig. S4), such as CO ($R = 0.6$) and NO_2 ($R = 0.5$),

226 and also tracked with HOA ($R = 0.4$). These observations suggest that the primary-related-SOA
227 might be transformed from locally emitted POA as a non-negligible source to SOA.

228 To further investigate the SOA formation mechanism, the dataset was segregated into three
229 periods according to different features depends on meteorological parameters (Fig. 2), i.e., the
230 reference period (P1), high- O_x period (P2) and high-RH period (P3). Briefly, the reference
231 period, P1, was characterized by a low average OA concentration ($15.4 \pm 3.2 \mu\text{g m}^{-3}$) and was
232 mainly affected by clean air from southwest of the sampling site and precipitation activities
233 (Table S1). The high- O_x period (P2) was featured by a high O_x concentration (65.1 ± 20.4 ppb),
234 warmer temperatures (26.4 ± 4.0 °C) but lower RH (57.7 ± 17.5 %). The mass loadings of OA
235 ($19.8 \pm 4.7 \mu\text{g m}^{-3}$) and other pollutants in P2 were higher than those in P1 (Table S1). P3 was
236 assigned as a high-RH period because of the noticeably high RH (83.7 ± 12.5 %) and high
237 ALWC ($95.4 \pm 114.2 \mu\text{g m}^{-3}$). Winds were weak ($<1.0 \text{ m s}^{-1}$) throughout this period, indicative
238 of stagnant conditions, which facilitated pollutant accumulation and resulted in the highest
239 average OA concentrations ($25.0 \pm 6.2 \mu\text{g m}^{-3}$).

240 During the reference period (P1), SOA had the lowest contribution to OA (57%), and the O_x -
241 initiated-SOA and aq-SOA constituted 22% and 21% to total OA, respectively. For the high-
242 O_x period (P2), enhanced SOA formation was found, with the SOA fraction increased to 71%
243 of the total OA. The ~~photochem-SOA~~ O_x -initiated-SOA showed the highest mass loading of 7.3
244 $\mu\text{g m}^{-3}$ and highest contribution of 37% to total OA. These increases suggest that high- O_x
245 condition facilitates the production of SOA by photochemistry, making the ~~photochem-SOA~~ O_x -
246 initiated-SOA the major source of SOA during P2. During the high-RH period (P3), SOA
247 fraction continually increased, approaching 79% in total OA, and the SOA was mainly
248 contributed by aq-SOA and fresh-SOA. The mass contribution of aq-SOA increased
249 dramatically from 9% to total OA during P2 to 33% during P3 (Fig. S2), and average mass
250 concentrations from $1.8 \mu\text{g m}^{-3}$ to $8.3 \mu\text{g m}^{-3}$, which suggests rapid SOA production through the
251 aqueous-phase chemistry. Comparatively, the contribution of fresh-SOA was about ~20% in
252 both P2 and P3, but lower in P1 (9%), suggesting that the formation fresh-SOA was affected
253 by both high O_x and high RH. It should also be noted that O:C ratio increased in the succession
254 from P1 (0.73) to P2 (0.74) and further to P3 (0.77), accompanied by continually decrease of
255 H:C ratio from 1.64 to 1.56, and to 1.53 (Fig. 3), suggesting the increase of OA oxidation degree.
256 As a result, the high O_x in P2 and high RH in P3 (as compared to P1) promoted the formation
257 of SOA, specifically ~~photochem-SOA~~ O_x -initiated-SOA (in P2) and aq-SOA (in P3), leading to
258 the increase in the degree of oxygenation in total OA.

259 ~~Although the primary related SOA constituted a small fraction and showed little variation~~
260 ~~during P1-P3 (3%~5%), this SOA source is also of particular interest because of its distinctive~~
261 ~~fragments with high m/z values in the mass spectrum (Fig. 1d). At $m/z < 120$, the primary-~~

262 related SOA had higher intensities for m/z 43 (mainly $C_2H_3O^+$) and m/z 44 (mainly CO_2^+) than
263 those in POA, indicating a typical nature of less oxidized SOA. At $m/z > 120$, PAH derived
264 fragments are clearly evident in the mass spectrum of the primary related SOA, as indicated by
265 PAH like ions at m/z 152, 165, 178, 189, 202, 216, 226 + 228, 240 + 242, 250 + 252, 264 +
266 266, and 276 + 278 (Dzepina et al., 2007). Previous AMS studies have observed pronounced
267 peaks of PAH ions in POA mass spectra, such as those in coal combustion organic aerosol
268 (CCOA) and biomass burning organic aerosol (BBOA) (Hu et al., 2016b; Zhao et al., 2019),
269 but rarely in SOA. This observation implies that the primary related SOA may be related to the
270 POA originated from domestic coal combustion (Xu et al., 2006). Moreover, this SOA factor
271 exhibited relatively better correlations with some gaseous pollutants (Fig. S4), such as CO (R
272 = 0.6) and NO_2 ($R = 0.5$), and also tracked with HOA ($R = 0.4$). These observations suggest
273 that the primary related SOA might be transformed from locally emitted POA as a non-
274 negligible source to SOA. Overall, our results suggest that SOA could be formed through
275 different pathways, in particular photochemistry, aqueous-phase chemistry, and conversion of
276 POA to SOA contributed to SOA formation.

277 3.2 Photochemistry

278 As expected for summertime, photochemistry associated with O_x has significant impacts on
279 the formation and evolution of SOA. Herein, the relationships between OA factors and O_x were
280 investigated to offer insights into the formation mechanisms of SOA associated with the ozone
281 production chemistry (Herndon et al., 2008). During P2, as O_x increased, the mass loadings of
282 ~~photochem SOA~~ O_x -initiated-SOA showed a substantially increasing trend when O_x was > 30 ppb
283 and eventually saturated when O_x was > 100 ppb, raising the contribution of ~~photochem SOA~~ O_x -
284 initiated-SOA from 20% to 61% of total OA (Fig. 4). This observation indicates the importance
285 of photochemistry in the formation of ~~photochem SOA~~ O_x -initiated-SOA in summer, in which
286 high O_x concentration as well as temperature corresponding to strong atmospheric oxidative
287 capacity, can accelerate the photochemical formation (Duan et al., 2021). As a comparison, the
288 mass concentrations of other OA factors except ~~photochem SOA~~ O_x -initiated-SOA showed
289 decreasing trends as O_x increased (Fig. 4c). Such differences between SOA factors are likely
290 due to the enhanced secondary production/transformation from POA and fresher SOA factors
291 to the more aged ~~photochem SOA~~ O_x -initiated-SOA. Note that the O:C ratio presented a faster
292 increasing rate as a function of O_x (from 0.6 to 1.0, Fig. 4d) than those in P1 and P3, suggesting
293 that photochemistry might result in higher OA oxidation state during P2.

294 The typical episode with high- O_x period (P2) was dominated by a series of daytime
295 photochemical evolutions. To evaluate the relative contributions of photochemical and
296 aqueous-phase processing production and the transformation of these SOA factors in different

297 meteorological stages, the average diurnal variations of OA factors, O:C ratios, O_x, temperature,
298 AWLC and primary gas pollutants and RH during different periods are shown for comparison.
299 Fig. 6 shows that O_x increased rapidly from 6:00 to 14:00 in all periods, but was highest in
300 P2. Correspondingly, a lower mean value of ALWC (8.4 μg m⁻³) was also observed in P2 than
301 in P1 and P3. These results are consistent with the increasing trend of T, and similar with
302 ultraviolet radiation in the result in (Li et al., (2020), a driver of photochemical activities,
303 suggesting that the oxidation of OA was enhanced at noon due to photochemical processing.
304 During P2, O_x-initiated-SOA was produced quickly and played the dominant role during
305 daytime, while its concentration typically decreased during nighttime. The average
306 concentration of ~~photochem-SOA~~O_x-initiated-SOA increased continually from 4.2 μg m⁻³ at 7:00
307 local time (LT) to 10.4 μg m⁻³ at 15:00 LT in 8 h, with the maximum ~~photochem-SOA~~O_x-
308 initiated-SOA mass fraction in OA reaching 65% at 15:00 LT (Fig. S6c). This high average
309 growth rate of 0.8 μg m⁻³ h⁻¹ in ~~photochem~~-O_x-initiated-SOA corresponded to the high O_x
310 concentration, high temperature and strong solar radiation in daytime, suggesting enhanced
311 photochemistry reaction. In contrast, the concentrations and the contributions of other SOA
312 factors decreased continuously at the same time (Fig. 6). The opposite trends between O_x-
313 initiated-SOA and other OA factors from 7:00 to 15:00 LT suggest that some part of POA and
314 fresh-SOA may convert to O_x-initiated-SOA by photochemical oxidation. This conclusion is
315 consistent with findings reported by Li et al., (2020) in urban Beijing, where less-oxidized SOA
316 may transform to more-oxidized SOA through photochemical processing as well. The O:C ratio
317 of OA presented a significant increasingly diurnal variation with a noon peak around 14:00 ~
318 16:00 LT in P2, which had the highest value of 0.74 compared with it in P1 and P3, suggesting
319 the potential transformation from POA factors and fresh SOA factors to ~~photochem-SOA~~ O_x-
320 initiated-SOA could also noticeably affect OA characteristics such as oxidation state in summer
321 daytime. The O:C ratio of OA also presented a significant increasingly diurnal variation with a
322 noon peak around 14:00 ~ 16:00 in P2, which had the highest value of 0.74 compared with it
323 in P1 and P3. It is further indicated by a small afternoon peak of the more oxidized tracer CO₂⁺
324 (m/z 44) and the decrease in a less oxidized tracer C₂H₃O⁺ (m/z 43) (Fig. 7b). As a result, the
325 mass spectra, which were initially fresh SOA products evolved to become aged SOA products
326 as the photochemical age increased. Overall, with little water in the particles, the high solar
327 radiation and high O_x concentration during daytime associated with a relatively high degree of
328 oxygenation of OA suggest that gas-phase oxidation and partitioning processes are probably
329 the dominating process in SOA formation during P2.

330 In addition, these results further support the idea that during the high-O_x period of summer,
331 photochemistry has significant impacts on SOA formation, especially on ~~photochem~~-O_x-initiated-
332 SOA. Note that the role of photochemistry in the formation of ~~photochem~~-O_x-initiated-SOA is
333 not only limited to the gas-phase photochemistry, but also can also occur in the aqueous phase

334 (Kuang et al., 2020). This is the case for P3 in our study, which is discussed further in section
335 3.3 below.

336

337 3.3 Aqueous-phase chemistry

338 The aqueous-phase chemistry has imposed significant impacts on SOA formation during this
339 field campaign. To further explore the formation mechanism of SOA associated with aqueous-
340 phase chemistry, the relationships between different OA factors and ALWC were investigated.
341 During P3, the mass concentration of aq-SOA increased from $5 \mu\text{g m}^{-3}$ to $17 \mu\text{g m}^{-3}$, yet its
342 fraction showed a particularly pronounced rise from 22.5% to 52% of total OA when ALWC
343 increased from 0.3 to $200 \mu\text{g m}^{-3}$ (Fig. 5e and f). Note that there are still consistent mass
344 concentrations of aq-SOA even when ALWC is very low (data interval ranging from 0~40 μg
345 m^{-3}), which is due to that over 80% of ALWC mass concentration were loaded in the first
346 interval, leading to a higher mean value of aq-SOA mass concentration. Actually ALWC
347 showed quite low mass loading in most period time but increased dramatically during P3, yet
348 the time series of aq-SOA and ALWC were remarkably well correlated throughout the entire
349 campaign ($R=0.7$, Fig. S4) rather than a strong correlation observed only in P3. Note that the
350 strong correlation between aq-SOA and ALWC was not only observed in P3. Rather, the time
351 series of aq-SOA and ALWC were remarkably well correlated throughout the entire campaign
352 ($R=0.7$, Fig. S4). This general correlation further confirms the important role of aqueous-phase
353 chemistry in the formation of aq-SOA and characterized the aqueous-phase formation of aq-
354 SOA throughout the campaign rather than only in the high-RH event as shown in section 3.1
355 earlier. We also found that the concentration and fraction of aq-SOA became stable when
356 ALWC was $> 200 \mu\text{g m}^{-3}$, which is probably attributable to that the aq-SOA formation within
357 droplets was soon outweighed by the scavenging processes when RH was high enough ($> 95\%$).
358 ~~Fig. 5e shows that the fresh SOA has similar increasing trend with aq-SOA as ALWC increased,~~
359 ~~which suggests that aqueous-phase chemistry might have also played an important role in the~~
360 ~~formation of fresh SOA. The fresh SOA also increased slightly as O_x increased (Fig. 4e),~~
361 ~~suggesting that both the aqueous-phase chemistry and the photochemistry (including that in the~~
362 ~~aqueous phase) participated to produce fresh SOA simultaneously.~~ The O:C ratio shows an
363 obvious increase from 0.7 to around 0.85 when ALWC increases to $200 \mu\text{g m}^{-3}$, after which it
364 remains relatively stable (0.85) as the ALWC increases further (Fig. 5). These results suggest
365 that aqueous-phase chemistry can affect the oxidation degree of OA by changing SOA
366 composition, especially the enhanced contribution of aq-SOA. However, the growth rate of O:C
367 ratios as ALWC increases in P3 was lower than that in P2 (up to 1 as O_x increases). Also, the

368 correlation between O:C vs. O_x in P2 ($R=0.6$) was stronger than O:C vs. ALWC ($R=0.3$) (Fig.
369 S8). ~~This result illustrates that photochemistry is more efficient in elevating the oxidation~~
370 ~~degree of OA than is the aqueous-phase chemistry.~~

371 Fig. 6 illustrate the different types of aqueous-phase chemistry in daytime and nighttime.
372 ~~During the nighttime in P3, aqueous-phase oxidation was also enhanced during nighttime~~
373 ~~(19:00–07:00 LT). As shown in Fig. 6, O:C ratio (0.76) at nighttime in P3 was higher than those~~
374 ~~in P2, while exhibiting a much smaller peak during daytime. Compared with the low ALWC in~~
375 ~~P2, the much higher ALWC concentration (peak value of $235.9 \mu\text{g m}^{-3}$ at 2:00 LT) and higher~~
376 ~~RH (peak value of 93.7% at 6:00 LT) during nighttime in P3 suggested a dominant contribution~~
377 ~~by aqueous-phase processing. The aq-SOA shows a quite clear and unique diurnal pattern in~~
378 ~~P3, with much higher mass concentration during the whole day (especially at nighttime) than~~
379 ~~those in P1 and P2. After 17:00 LT, aq-SOA started to increase from $4.7 \mu\text{g m}^{-3}$ to $12.7 \mu\text{g m}^{-3}$~~
380 ~~at 7:00 LT, which showed a rapid nighttime growth rate of $0.6 \mu\text{g m}^{-3} \text{h}^{-1}$, indicating enhanced~~
381 ~~SOA formation through aqueous-phase chemistry at night. Whereas O_x -initiated-SOA~~
382 ~~decreased rapidly from $8.2 \mu\text{g m}^{-3}$ at 17:00 LT until reaching its lowest concentration of 2.6~~
383 ~~$\mu\text{g m}^{-3}$ until the morning, suggesting the gas-to-particle partitioning at night under high ALWC~~
384 ~~conditions. Furthermore, this transformation could be supported by the increase in CO_2^+ (m/z~~
385 ~~44) and the decrease in a less oxidized tracer $\text{C}_2\text{H}_3\text{O}^+$ (m/z 43) at night (Fig. 7c). Since –when~~
386 ~~the ALWC is sufficiently high, it was likely to accommodate much of the precursor organics~~
387 ~~and oxidants to low-volatility products through aqueous-phase oxidation. In addition, the dark~~
388 ~~aqueous-phase SOA formation was likely strong enough to counteract the nighttime scavenging~~
389 ~~processes under high-RH conditions. Therefore, the dark aqueous-phase chemistry forming aq-~~
390 ~~SOA shows a dominant role (over 40% to OA) during nighttime in P3.~~

391 ~~However, The aq-SOA shows a quite clear and unique diurnal pattern in P3, with much~~
392 ~~higher mass concentration during the whole day (especially at nighttime) than those in P1 and~~
393 ~~P2. This may be attributed to the stagnant meteorological conditions and high RH (thus ALWC),~~
394 ~~which facilitated the continuous formation of aq-SOA in P3. during the daytime, the mass~~
395 ~~concentration of aq-SOA decreased from 7:00 to 17:00 LT in P3, coinciding an obvious~~
396 ~~increase trend of O_x -initiated-SOA at the same time with an average growth rate of $0.6 \mu\text{g m}^{-3}$~~
397 ~~h^{-1} (Fig. 6). This phenomenon suggests photochemical processing can also occur in the aqueous~~
398 ~~phase when RH and ALWC were still high, consistent with the decrease of RH and the increase~~
399 ~~of temperature (Fig. 6S7). WIn addition, we also noticed that significant phochem SOA~~
400 ~~O_x -initiated-SOA formation also occurred during daytime in P3 with an average growth rate of~~
401 ~~$0.6 \mu\text{g m}^{-3} \text{h}^{-1}$. This observation is similar to results in a previous study showing that both~~
402 ~~aqueous phase and gas phase photochemical reactions substantially contributed to the~~
403 ~~formation of OOA (a surrogate of SOA) during the high RH period (Kuang et al., 2020). The~~

404 rapid daytime photochem SOA formation in our study probably occurred in the aqueous phase
405 driven by photochemical reactions during daytime under humid conditions with high ALWC.
406 The O_x initiated SOA increased from 2.6 μg m⁻³ at 7:00 LT until reaching its highest
407 concentration of 8.2 μg m⁻³ at 16:00 LT with an average growth rate of 0.6 μg m⁻³h⁻¹ and then
408 decreased rapidly until night, coinciding with obvious decrease trend of aq SOA at the same
409 time. This distinct trends further suggest that the transformation of gas particle partitioning
410 through aqueous phase chemistry at daytime. Photochemical reactions through both aqueous-
411 phase and gas-phase can contribute substantially to the SOA formation in polluted areas of NCP,
412 and during haze days with high RH and ALWC the aqueous-phase photochemical processes
413 played a dominant role in daytime SOA formation (Kuang et al., 2020). The rapid daytime O_x-
414 initiated-SOA formation in our study possibly occurred on the particle surface and in the aerosol
415 liquid water (Ervens et al., 2011) under humid conditions with high ALWC but driven by gas-
416 phase direct photolysis and oxidation by photooxidants under high O_x conditions. Under such
417 high-RH level (RH > 80%), the water-soluble species produced from photochemistry in the gas
418 phase can also partition into the aqueous phase and be further oxidized to form low-volatility
419 products (Carlton et al., 2007; Sullivan et al., 2016). Previous studies have demonstrated that
420 gas-phase oxidants such as OH radicals and H₂O₂ can also partition to the aqueous phase to
421 further oxidize dissolved the oxidized VOCs (OVOCs) into aq-SOA (Ye et al., 2018). Other
422 studies also revealed that photochemical reactions in the aqueous droplets can occur through
423 direct photolysis or through oxidation by oxidants (Ervens et al., 2011; 2014; Ye et al., 2018).
424 Therefore, in our campaign, dark aqueous-phase chemistry is responsible for rapid aq-SOA
425 formation during nighttime, while the aqueous-phase photochemistry during daytime is likely
426 prevail by rapid daytime photochem- O_x-initiated-SOA formation during P3. This comparison
427 demonstrates that the nocturnal aqueous-phase chemistry and daytime aqueous-phase
428 photochemistry are both important pathways in the total SOA growth.

429 The aqueous-phase chemistry related to fresh-SOA is more complicated, requiring both
430 daytime radiative conditions and certain amounts of ALWC in nighttime. For example, Fig. 5e
431 shows that the fresh-SOA has a similar increasing trend with aq-SOA as ALWC increased,
432 however, it also increased slightly as O_x increased (Fig. 4e), hinting that both ALWC and the
433 oxidants are critical for fresh-SOA formation and both the aqueous-phase chemistry and the
434 photochemistry (including that in the aqueous phase) participated to produce fresh-SOA
435 simultaneously. It is worth noting that three peaks were found in the diurnal variation of fresh-
436 SOA in P3. The peaks at around 6:00 and 19:00 LT at night were similar to those of aq-SOA
437 and lower than it, while the peak at around 13:00 LT is consistent with the peak in the diurnal
438 cycle of O_x (Fig. 6). Although there is also a smaller peak around 13:00 LT in P3, the whole
439 pattern of aq-SOA is characterized by decreasing trend at daytime. These results suggest that
440 fresh-SOA could be formed through dark nighttime aqueous-phase reactions, which are

441 partially reversible upon the evaporation of aerosol liquid water, and also formed through
442 photochemical aqueous-phase reactions during daytime. Different from aq-SOA, which is
443 highly correlated and limited with ALWC, two types of aqueous-phase chemistry in daytime
444 and nighttime are dominant pathways to the fresh-SOA growth. This three-peak diurnal pattern
445 hints that both the dark aqueous phase chemistry and the daytime photochemistry (either in the
446 gas phase or in the aqueous phase) are important in the formation of fresh SOA. Our analysis
447 on formation pathways of these SOA factors suggested the potential interactive roles of gas-
448 phase oxidation, gas-particle partitioning, and aqueous-phase oxidation in the formation of
449 SOA.

450 3.4 SOA from POA transformation

451 The photochemistry and aqueous-phase chemistry show distinct effects on POA evolution
452 and SOA formation. The relationships between ~~photochem-SOA~~ O_x -initiated-SOA /aq-SOA and
453 other POA-related components (HOA + COA + primary-related-SOA) were plotted in Fig. S9.
454 A strong negative correlation ($R=-0.8$) between POA-related components and ~~photochem-SOA~~
455 O_x -initiated-SOA was observed (Fig. S9c), consistent with the decrease in mass concentration
456 of POA-related components during P2. This observation suggests that the production of
457 ~~photochem-SOA~~ O_x -initiated-SOA was at least partly facilitated by photochemical transformation
458 of other OA components. ~~However, the better diffusion conditions in P2 might also attribute a~~
459 ~~great extent to the negative correlation, as the formation period of O_x -initiated-SOA usually~~
460 ~~occurred during the noontime when the boundary layer was much developed, while the POA~~
461 ~~usually decreased via horizontal and vertical diffusion. In addition, compared with P1 and P3,~~
462 ~~a more positive promotion on the photochem-SOA O_x initiated SOA formation was observed in~~
463 ~~P2 when O_x was more than 40 ppb. These observations confirm the results in section 3.2 that~~
464 ~~intensive formation of photochem-SOA O_x initiated SOA was not only produced by~~
465 ~~photochemical oxidation from VOCs at high O_x levels, but also potentially through the~~
466 ~~transformation of POA related components into photochem-SOA O_x initiated SOA. In~~
467 comparison, POA-related components and aq-SOA correlate weakly. When ALWC ($<20 \mu\text{g}$
468 m^{-3}) and nitrate concentrations were lower ($<3 \mu\text{g} \text{m}^{-3}$), mostly during P1 and P2, POA-related
469 components and aq-SOA showed almost no correlation ($R=0.1$ and $R=-0.1$). However, when
470 ALWC concentration and nitrate concentration were higher than those thresholds above (data
471 points with yellow/red colors mostly during P3), they had a relatively good negative correlation
472 ($R=-0.5$) (Fig. S9f), indicating the importance of ALWC and nitrate in aqueous-phase chemistry.
473 This is consistent with results in winter Beijing (Wang et al., 2021), where POA factor had
474 strong negative correlations with aq-SOA, suggesting that these POA factors might produce aq-
475 SOA by aqueous-phase oxidation. In addition, under high-ALWC conditions, nitrate had
476 similar formation mechanisms with aq-SOA or high nitrate supports the potential

477 formation/transformation from POA-related components to aq-SOA, which is consistent with
478 the results in section 3.3. The phenomenon of negative correlation between POA-related
479 components and SOA at high $O_x/ALWC$ further emphasizes the importance of conversion from
480 POA to SOA.

481 As shown in the Van Krevelen (VK) plot (Fig. 8a), O:C and H:C both increase in the
482 succession from primary-related-SOA to ~~photochem-SOA~~ O_x -initiated-SOA and eventually to aq-
483 SOA, supporting a successive oxidation sequence from primary-related-SOA to aq-SOA.
484 Generally, H:C shows a decreasing trend as O:C increases for organic compounds during
485 oxidation in other studies (Ng et al., 2011; Gilardoni et al., 2016; Lee et al., 2017; Zhao et al.,
486 2019; Chen et al., 2021), suggesting a general negative correlation between H:C and O:C. This
487 positive relationship of O:C and H:C evolution during oxidative aging in this study is interesting.
488 It might be caused by ring-breaking reactions which could further promote the transformation
489 of aromatic POA to aq-SOA. Previous studies in both laboratory (Huang et al., 2018; Wang et
490 al., 2020) and field (Hu et al., 2016a) demonstrated that the OH-initiated ring-breaking reactions
491 of aromatic species can occur in the aqueous phase and form highly oxidized oxygenated
492 compounds. For example, Hems and Abbatt (2018) suggested that nitrophenol molecules could
493 react rapidly with OH radicals in aqueous solutions with the addition of OH functional groups
494 to the aromatic ring at the initial stage, followed by fragmentation to multifunctional organic
495 species with high H:C and O:C ratios. Wang et al. (2021) found that the ring-breaking oxidation
496 of aromatic FF-POA was the mechanism for aq-SOA formation. Similar to those in primary-
497 related-SOA, PAH-like ions was also found in the mass spectrum of aq-SOA at $m/z > 150$,
498 albeit less pronounced, consistent with a previous study in Beijing (Wang et al., 2021). This is
499 likely due to the oxidation of PAHs in the conversion of primary-related-SOA and aq-SOA,
500 which is caused by enhanced hydroxylation of the aromatic ring and increased yields of
501 carboxylic acids in OH-initiated reactions (Sun et al., 2010). This kind of ring-breaking
502 oxidation of aromatic POA could thus lead to aq-SOA formation (Huang et al., 2018; Wang et
503 al., 2021). In addition, the locations of aq-SOA and the slope of overall OA are near the line
504 with the slope of -1 in the VK plot, indicating more carboxylic acid formation while the
505 replacement of a hydrogen atom with a carboxylic acid group ($-COOH$) (Heald et al., 2010;
506 Ng et al., 2011). This observation supports that oxidation of PAHs was probably involved in
507 the conversion of primary-related-SOA to aq-SOA through aqueous-phase chemistry, leading
508 to functionalization as carbonyls and carboxylic acids.

509 Specifically, the organic fragments and mass spectrum evolution of OA were analyzed to
510 illuminate the transformation in photochemical processing and aqueous-phase chemistry. Fig.
511 8b shows the mass fractions of $CH_2O_2^+$, CH_3SO^+ , HCO_2^+ , and $C_2H_2O_2^+$ ion fragments in OA as
512 a function of ALWC. The aq-SOA was tightly correlated with $CH_2O_2^+$ ($R^2 = 0.81$) at m/z 46

513 and CH_3SO ($R^2 = 0.78$) at m/z 63 (Fig. S10), Consistently, both of them showed increase trends
514 as ALWC increasing, similar as aq-SOA, which indicating typical fragment characteristics of
515 ions of aqueous-phase processing products (Tan et al., 2009; Sun et al., 2016; Duan et al., 2021).
516 The intensities of HCO_2^+ (m/z 45), a common fragment ion of carboxylic acids, is associated
517 with aqueous oxidation of aromatic compounds. $\text{C}_2\text{H}_2\text{O}_2^\pm$ (m/z 58) is a tracer ion for glyoxal,
518 which could be a ring-breaking product from the aqueous-phase oxidation of PAHs. The
519 increasing trends of these ions with ALWC suggest that water-soluble organic species such as
520 carboxylic acids and glyoxal are produced as components of aq-SOA following aromatic
521 oxidation and ring breaking. Moreover, the concentration of PAHs increased with the increase
522 of ALWC (Fig. S11), consistent with the oxidation of PAHs from ring-breaking reactions that
523 can take place in the aqueous phase and being involved in the conversion to aq-SOA.

524 4. Conclusion

525 The sources and formation mechanisms of SOA were investigated by online aerosol mass
526 spectrometry and statistical (PMF) analysis from August to September of 2019 in Handan, a
527 mid-sized industrialized city in NCP of China. Four specific SOA factors were resolved,
528 including aq-SOA (15% to total OA), ~~photochem-SOA~~ O_x -initiated-SOA (31%), fresh-SOA (18%)
529 and primary-related-SOA (5%). By studying the formation of these SOA factors in different
530 selected periods (P1-P3) against O_x and ALWC, we found multiple pathways leading to their
531 formation, sometimes with mixed pathways for one type of SOA.

532 Both photochemistry and aqueous-phase chemistry resulted in enhanced OA oxidation state,
533 ~~but the effect of photochemistry was stronger in SOA formation.~~ During high- O_x period,
534 photochemistry had imposed significant impacts on the formation and evolution of SOA in
535 summertime. The ~~photochem-SOA~~ O_x -initiated-SOA contributed up to 65% to total OA in the
536 daytime, with a high average growth rate of $0.8 \mu\text{g m}^{-3} \text{h}^{-1}$, suggesting the efficient daytime
537 formation of SOA from photochemistry. Rapid increases of the concentration and contribution
538 (up to 61%) of ~~photochem-SOA~~ O_x -initiated-SOA were found as O_x increased, while all the other
539 OA factors showed decreasing trends with O_x concentration increasing. The difference suggests
540 enhanced secondary transformation from POA/fresh SOA factors to the more aged ~~photochem-~~
541 ~~SOA~~ O_x -initiated-SOA under high- O_x condition. However, during the high-RH period, two
542 types of aqueous-phase chemistry were both important pathways for the SOA growth. During
543 nighttime and under high-RH conditions, dark aqueous-phase chemistry played significant
544 roles with rapid aq-SOA formation (up to 45% in total OA), while the aqueous-phase
545 photochemistry was more important by rapid ~~photochem-SOA~~ O_x -initiated-SOA formation
546 during daytime (up to 39% in total OA). The primary-related-SOA was evidently linked to the
547 POA originated from coal combustion activities, as indicated by the PAH-like ion peaks.
548 Although it constituted a small fraction of 5%, the potential transformation and conversion from

549 primary-related-SOA to aq-SOA could also be an important pathway via hydroxylation of the
550 aromatic ring or ring-breaking oxidation of aromatic POA species through aqueous-phase
551 chemistry. This study highlights the multiple reaction pathways, on top of multiple precursor
552 types, on the SOA formation in industrialized regions, and calls for more in-depth study on
553 the interactive roles of those formation pathways.

554

555 **Data availability.** Raw data used in this study are archived at the Institute of Earth Environment,
556 Chinese Academy of Sciences, and are available on request by contacting the corresponding
557 author.

558 **Supplement.** The Supplement related to this article is available online.

559 **Competing interests.** The authors declare that they have no conflict of interest.

560 **Author contributions.** RJH designed the study. Data analysis and source apportionment were
561 done by YFG and RJH. YFG and RJH wrote the manuscript. YFG and RJH interpreted data
562 and prepared display items. All authors commented on and discussed the manuscript.

563 **Acknowledgement**

564 This work was supported by the National Natural Science Foundation of China (no.
565 41925015), the Key Research Program of Frontier Sciences from the Chinese Academy of
566 Sciences (no. ZDBS-LY-DQC001), the Strategic Priority Research Program of the Chinese
567 Academy of Sciences (no. XDB40000000), and SKLLQG (no. SKLLQGTD1801).

568

569 **References**

570 An, Z., Huang, R. J., Zhang, R., Tie, X., Li, G., Cao, J., Zhou, W., Shi, Z., Han, Y., Gu, Z., and
571 Ji, Y.: Severe haze in northern China: A synergy of anthropogenic emissions and
572 atmospheric processes, *Proc. Natl. Acad. Sci. U. S. A.*, 116, 8657–8666,
573 <https://doi.org/10.1073/pnas.1900125116>, 2019.

574 Bikkina, S., Kawamura, K., and Sarin, M.: Secondary Organic Aerosol Formation over Coastal
575 Ocean: Inferences from Atmospheric Water-Soluble Low Molecular Weight Organic
576 Compounds, *Environ. Sci. Technol.*, 51, 4347–4357,
577 <https://doi.org/10.1021/acs.est.6b05986>, 2017.

578 Canagaratna, M. R., Jimenez, J. L., Kroll, J. H., Chen, Q., Kessler, S. H., Massoli, P.,
579 Hildebrandt Ruiz, L., Fortner, E., Williams, L. R., Wilson, K. R., Surratt, J. D., Donahue, N.
580 M., Jayne, J. T., and Worsnop, D. R.: Elemental ratio measurements of organic compounds
581 using aerosol mass spectrometry: Characterization, improved calibration, and implications,
582 *Atmos. Chem. Phys.*, 15, 253–272, <https://doi.org/10.5194/acp-15-253-2015>, 2015.

583 Canonaco, F., Crippa, M., Slowik, J. G., Baltensperger, U., and Prévôt, A. S. H.: SoFi, an
584 IGOR-based interface for the efficient use of the generalized multilinear engine (ME-2) for
585 the source apportionment: ME-2 application to aerosol mass spectrometer data, *Atmos.*
586 *Meas. Tech.*, 6, 3649–3661, <https://doi.org/10.5194/amt-6-3649-2013>, 2013.

587 Carlton, A. G., Turpin, B. J., Altieri, K. E., Seitzinger, S., Reff, A., Lim, H. J., and Ervens, B.:
588 Atmospheric oxalic acid and SOA production from glyoxal: Results of aqueous
589 photooxidation experiments, *Atmos. Environ.*, 41, 7588–7602,
590 <https://doi.org/10.1016/j.atmosenv.2007.05.035>, 2007.

591 Chen, W., Ye, Y., Hu, W., Zhou, H., Pan, T., Wang, Y., Song, W., Song, Q., Ye, C., Wang, C.,
592 Wang, B., Huang, S., Yuan, B., Zhu, M., Lian, X., Zhang, G., Bi, X., Jiang, F., Liu, J.,
593 Canonaco, F., Prevot, A. S. H., Shao, M., and Wang, X.: Real-time characterization of
594 aerosol compositions, sources and aging processes in Guangzhou during PRIDE-GBA 2018
595 campaign, *J. Geophys. Res. Atmos.*, <https://doi.org/10.1029/2021jd035114>, 2021.

596 Cohen, A. J., Brauer, M., Burnett, R., Anderson, H. R., Frostad, J., Estep, K., Balakrishnan, K.,
597 Brunekreef, B., Dandona, L., Dandona, R., Feigin, V., Freedman, G., Hubbell, B., Jobling,
598 A., Kan, H., Knibbs, L., Liu, Y., Martin, R., Morawska, L., Pope, C. A., Shin, H., Straif, K.,
599 Shaddick, G., Thomas, M., van Dingenen, R., van Donkelaar, A., Vos, T., Murray, C. J. L.,
600 and Forouzanfar, M. H.: Estimates and 25-year trends of the global burden of disease
601 attributable to ambient air pollution: an analysis of data from the Global Burden of Diseases
602 Study 2015, *Lancet*, 389, [https://doi.org/10.1016/S0140-6736\(17\)30505-6](https://doi.org/10.1016/S0140-6736(17)30505-6), 2017.

603 Donahue, N. M., Robinson, A. L., Stanier, C. O., and Pandis, S. N.: Coupled partitioning,
604 dilution, and chemical aging of semivolatile organics, *Environ. Sci. Technol.*, 40,
605 <https://doi.org/10.1021/es052297c>, 2006.

- 606 Duan, J., Huang, R. J., Gu, Y., Lin, C., Zhong, H., Wang, Y., Yuan, W., Ni, H., Yang, L., Chen,
607 Y., Worsnop, D. R., and O'Dowd, C.: The formation and evolution of secondary organic
608 aerosol during summer in Xi'an: Aqueous phase processing in fog-rain days, *Sci. Total*
609 *Environ.*, 756, 144077, <https://doi.org/10.1016/j.scitotenv.2020.144077>, 2021.
- 610 Dzepina, K., Arey, J., Marr, L. C., Worsnop, D. R., Salcedo, D., Zhang, Q., Onasch, T. B.,
611 Molina, L. T., Molina, M. J., and Jimenez, J. L.: Detection of particle-phase polycyclic
612 aromatic hydrocarbons in Mexico City using an aerosol mass spectrometer, *Int. J. Mass*
613 *Spectrom.*, 263, 152–170, <https://doi.org/10.1016/j.ijms.2007.01.010>, 2007.
- 614 Elser, M., Huang, R., Wolf, R., Slowik, J. G., Wang, Q., Canonaco, F., Li, G., Bozzetti, C.,
615 Daellenbach, K. R., Huang, Y., Zhang, R., Li, Z., Cao, J., Baltensperger, U., El-haddad, I.,
616 and Prévôt, A. S. H.: New insights into PM_{2.5} chemical composition and sources in two
617 major cities in China during extreme haze events using aerosol mass spectrometry, 3207–
618 3225, <https://doi.org/10.5194/acp-16-3207-2016>, 2016.
- 619 Ervens, B., Turpin, B. J., and Weber, R. J.: Secondary organic aerosol formation in cloud
620 droplets and aqueous particles (aqSOA): A review of laboratory, field and model studies,
621 *Atmos. Chem. Phys.*, 11, 11069–11102, <https://doi.org/10.5194/acp-11-11069-2011>, 2011.
- 622 Ervens, B., Armin, S., B., L. Y., and J., and T. B.: Key parameters controlling OH-initiated
623 formation of secondary organic aerosol in the aqueous phase (aqSOA), *J. Geophys. Res.*,
624 6578–6595, <https://doi.org/10.1002/2013JD021021>.Received, 2014.
- 625 Fountoukis, C. and Nenes, A.: ISORROPIAII: A computationally efficient thermodynamic
626 equilibrium model for K⁺-Ca²⁺-Mg²⁺-NH₄⁺-Na⁺-SO₄²⁻-NO₃⁻-Cl⁻-H₂O aerosols, *Atmos.*
627 *Chem. Phys.*, 7, 4639–4659, <https://doi.org/10.5194/acp-7-4639-2007>, 2007.
- 628 Gilardoni, S., Massoli, P., Paglione, M., Giulianelli, L., Carbone, C., Rinaldi, M., Decesari, S.,
629 Sandrini, S., Costabile, F., and Gobbi, G. P.: Direct observation of aqueous secondary
630 organic aerosol from biomass-burning emissions, *Proc. Natl. Acad. Sci. U. S. A.*, 113,
631 10013–10018, <https://doi.org/10.1073/pnas.1602212113>, 2016.
- 632 Gu, Y., Huang, R. J., Li, Y., Duan, J., Chen, Q., Hu, W., Zheng, Y., Lin, C., Ni, H., Dai, W.,
633 Cao, J., Liu, Q., Chen, Y., Chen, C., Ovadnevaite, J., Ceburnis, D., and O'Dowd, C.:
634 Chemical nature and sources of fine particles in urban Beijing: Seasonality and formation
635 mechanisms, *Environ. Int.*, 140, 105732, <https://doi.org/10.1016/j.envint.2020.105732>,
636 2020.
- 637 Heald, C. L., Kroll, J. H., Jimenez, J. L., Docherty, K. S., Decarlo, P. F., Aiken, A. C., Chen,
638 Q., Martin, S. T., Farmer, D. K., and Artaxo, P.: A simplified description of the evolution
639 of organic aerosol composition in the atmosphere, *Geophys. Res. Lett.*, 37,
640 <https://doi.org/10.1029/2010GL042737>, 2010.
- 641 Hems, R. F. and Abbatt, J. P. D.: Aqueous Phase Photo-oxidation of Brown Carbon
642 Nitrophenols: Reaction Kinetics, Mechanism, and Evolution of Light Absorption, *ACS*
643 *Earth Sp. Chem.*, 2, 225–234, <https://doi.org/10.1021/acsearthspacechem.7b00123>, 2018.

- 644 Hennigan, C. J., Izumi, J., Sullivan, A. P., Weber, R. J., and Nenes, A.: A critical evaluation of
645 proxy methods used to estimate the acidity of atmospheric particles, *Atmos. Chem. Phys.*,
646 15, 2775–2790, <https://doi.org/10.5194/acp-15-2775-2015>, 2015.
- 647 Herndon, S. C., Onasch, T. B., Wood, E. C., Kroll, J. H., Canagaratna, M. R., Jayne, J. T.,
648 Zavala, M. A., Knighton, W. B., Mazzoleni, C., Dubey, M. K., Ulbrich, I. M., Jimenez, J.
649 L., Seila, R., de Gouw, J. A., de Foy, B., Fast, J., Molina, L. T., Kolb, C. E., and Worsnop,
650 D. R.: Correlation of secondary organic aerosol with odd oxygen in Mexico City, *Geophys.*
651 *Res. Lett.*, 35, <https://doi.org/10.1029/2008GL034058>, 2008.
- 652 Hu, W., Hu, M., Hu, W. W., Niu, H., Zheng, J., Wu, Y., Chen, W., Chen, C., Li, L., Shao, M.,
653 Xie, S., and Zhang, Y.: Characterization of submicron aerosols influenced by biomass
654 burning at a site in the Sichuan Basin, southwestern China, *Atmos. Chem. Phys.*, 16, 13213–
655 13230, <https://doi.org/10.5194/acp-16-13213-2016>, 2016a.
- 656 Hu, W., Hu, M., Hu, W., Jimenez, J. L., Yuan, B., Chen, W., Wang, M., Wu, Y., Chen, C.,
657 Wang, Z., Peng, J., Zeng, L., and Shao, M.: *Journal of Geophysical Research : Atmospheres*,
658 1955–1977, <https://doi.org/10.1002/2015JD024020>.Received, 2016b.
- 659 Hu, W., Palm, B. B., Day, D. A., Campuzano-Jost, P., Krechmer, J. E., Peng, Z., De Sa Suzane,
660 S., Martin, S. T., Alexander, M. L., Baumann, K., Hacker, L., Kiendler-Scharr, A., Koss, A.
661 R., De Gouw, J. A., Goldstein, A. H., Seco, R., Sjostedt, S. J., Park, J. H., Guenther, A. B.,
662 Kim, S., Canonaco, F., Prévôt, A. S. H., Brune, W. H., and Jimenez, J. L.: Volatility and
663 lifetime against OH heterogeneous reaction of ambient isoprene-epoxydiols-derived
664 secondary organic aerosol (IEPOX-SOA), *Atmos. Chem. Phys.*, 16, 11563–11580,
665 <https://doi.org/10.5194/acp-16-11563-2016>, 2016c.
- 666 Hu, W., Hu, M., Hu, W., Zheng, J., Chen, C., Wu, Y., and Guo, S.: Seasonal variations in high
667 time-resolved chemical compositions, sources, and evolution of atmospheric submicron
668 aerosols in the megacity Beijing, 9979–10000, 2017.
- 669 Huang, D. D., Zhang, Q., Cheung, H. H. Y., Yu, L., Zhou, S., Anastasio, C., Smith, J. D., and
670 Chan, C. K.: Formation and Evolution of aqSOA from Aqueous-Phase Reactions of
671 Phenolic Carbonyls: Comparison between Ammonium Sulfate and Ammonium Nitrate
672 Solutions, *Environ. Sci. Technol.*, 52, 9215–9224, <https://doi.org/10.1021/acs.est.8b03441>,
673 2018.
- 674 Huang, R. J., Zhang, Y., Bozzetti, C., Ho, K. F., Cao, J. J., Han, Y., Daellenbach, K. R., Slowik,
675 J. G., Platt, S. M., Canonaco, F., Zotter, P., Wolf, R., Pieber, S. M., Bruns, E. A., Crippa,
676 M., Ciarelli, G., Piazzalunga, A., Schwikowski, M., Abbaszade, G., Schnelle-Kreis, J.,
677 Zimmermann, R., An, Z., Szidat, S., Baltensperger, U., El Haddad, I., and Prévôt, A. S. H.:
678 High secondary aerosol contribution to particulate pollution during haze events in China,
679 *Nature*, 514, 218–222, <https://doi.org/10.1038/nature13774>, 2014.
- 680 Huang, R. J., Wang, Y., Cao, J., Lin, C., Duan, J., Chen, Q., Li, Y., Gu, Y., Yan, J., Xu, W.,
681 Fröhlich, R., Canonaco, F., Bozzetti, C., Ovadnevaite, J., Ceburnis, D., Canagaratna, M. R.,
682 Jayne, J., Worsnop, D. R., El-Haddad, I., Prevot, A. S. H., and O’Dowd, C. D.: Primary

- 683 emissions versus secondary formation of fine particulate matter in the most polluted city
684 (Shijiazhuang) in North China, *Atmos. Chem. Phys.*, 19, 2283–2298,
685 <https://doi.org/10.5194/acp-19-2283-2019>, 2019.
- 686 Huang, R. J., He, Y., Duan, J., Li, Y., Chen, Q., Zheng, Y., Chen, Y., Hu, W., Lin, C., Ni, H.,
687 Dai, W., Cao, J., Wu, Y., Zhang, R., Xu, W., Ovadnevaite, J., Ceburnis, D., Hoffmann, T.,
688 and D. O'Dowd, C.: Contrasting sources and processes of particulate species in haze days
689 with low and high relative humidity in wintertime Beijing, *Atmos. Chem. Phys.*, 20, 9101–
690 9114, <https://doi.org/10.5194/acp-20-9101-2020>, 2020.
- 691 Jimenez, J. L., Jayne, J. T., Shi, Q., Kolb, C. E., Worsnop, D. R., Yourshaw, I., Seinfeld, J. H.,
692 Flagan, R. C., Zhang, X., Smith, K. A., Morris, J. W., and Davidovits, P.: Ambient aerosol
693 sampling using the Aerodyne aerosol mass spectrometer, *J. Geophys. Res. Atmos.*, 108, 1–
694 13, <https://doi.org/10.1029/2001jd001213>, 2003.
- 695 Jimenez, J. L., Canagaratna, M. R., Donahue, N. M., Prevot, A. S. H., Zhang, Q., Kroll, J. H.,
696 DeCarlo, P. F., Allan, J. D., Coe, H., Ng, N. L., Aiken, A. C., Docherty, K. S., Ulbrich, I.
697 M., Grieshop, A. P., Robinson, A. L., Duplissy, J., Smith, J. D., Wilson, K. R., Lanz, V. A.,
698 Hueglin, C., Sun, Y. L., Tian, J., Laaksonen, A., Raatikainen, T., Rautiainen, J., Vaattovaara,
699 P., Ehn, M., Kulmala, M., Tomlinson, J. M., Collins, D. R., Cubison, M. J., Dunlea, E. J.,
700 Huffman, J. A., Onasch, T. B., Alfarra, M. R., Williams, P. I., Bower, K., Kondo, Y.,
701 Schneider, J., Drewnick, F., Borrmann, S., Weimer, S., Demerjian, K., Salcedo, D., Cottrell,
702 L., Griffin, R., Takami, A., Miyoshi, T., Hatakeyama, S., Shimono, A., Sun, J. Y., Zhang,
703 Y. M., Dzepina, K., Kimmel, J. R., Sueper, D., Jayne, J. T., Herndon, S. C., Trimborn, A.
704 M., Williams, L. R., Wood, E. C., Middlebrook, A. M., Kolb, C. E., Baltensperger, U., and
705 Worsnop, D. R.: Evolution of organic aerosols in the atmosphere, *Science (80-)*, 326,
706 1525–1529, <https://doi.org/10.1126/science.1180353>, 2009.
- 707 Kuang, Y., He, Y., Xu, W., Yuan, B., Zhang, G., Ma, Z., Wu, C., Wang, C., Wang, S., Zhang,
708 S., Tao, J., Ma, N., Su, H., Cheng, Y., Shao, M., and Sun, Y.: Photochemical Aqueous-Phase
709 Reactions Induce Rapid Daytime Formation of Oxygenated Organic Aerosol on the North
710 China Plain, *Environ. Sci. Technol.*, 54, 3849–3860,
711 <https://doi.org/10.1021/acs.est.9b06836>, 2020.
- 712 Lee, A. K. Y., Chen, C. L., Liu, J., Price, D. J., Betha, R., Russell, L. M., Zhang, X., and Cappa,
713 C. D.: Formation of secondary organic aerosol coating on black carbon particles near
714 vehicular emissions, *Atmos. Chem. Phys.*, 17, 15055–15067, <https://doi.org/10.5194/acp-17-15055-2017>, 2017.
- 716 Li, H., Zhang, Q., Zhang, Q., Chen, C., Wang, L., Wei, Z., Zhou, S., Parworth, C., Zheng, B.,
717 Canonaco, F., Prévôt, A. S. H., Chen, P., Zhang, H., Wallington, T. J., and He, K.:
718 Wintertime aerosol chemistry and haze evolution in an extremely polluted city of the North
719 China Plain: Significant contribution from coal and biomass combustion, *Atmos. Chem.
720 Phys.*, 17, 4751–4768, <https://doi.org/10.5194/acp-17-4751-2017>, 2017.

- 721 Li, J., Liu, Z., Gao, W., Tang, G., Hu, B., Ma, Z., and Wang, Y.: Insight into the formation and
722 evolution of secondary organic aerosol in the megacity of Beijing, China, *Atmos. Environ.*,
723 220, <https://doi.org/10.1016/j.atmosenv.2019.117070>, 2020.
- 724 Middlebrook, A. M., Bahreini, R., Jimenez, J. L., and Canagaratna, M. R.: Evaluation of
725 composition-dependent collection efficiencies for the Aerodyne aerosol mass spectrometer
726 using field data, *Aerosol Sci. Technol.*, 46, 258–271,
727 <https://doi.org/10.1080/02786826.2011.620041>, 2012.
- 728 Ng, N. L., Canagaratna, M. R., Zhang, Q., Jimenez, J. L., Tian, J., Ulbrich, I. M., Kroll, J. H.,
729 Docherty, K. S., Chhabra, P. S., Bahreini, R., Murphy, S. M., Seinfeld, J. H., Hildebrandt,
730 L., Donahue, N. M., Decarlo, P. F., Lanz, V. A., Prévôt, A. S. H., Dinar, E., Rudich, Y., and
731 Worsnop, D. R.: Organic aerosol components observed in Northern Hemispheric datasets
732 from Aerosol Mass Spectrometry, *Atmos. Chem. Phys.*, 10, 4625–4641,
733 <https://doi.org/10.5194/acp-10-4625-2010>, 2010.
- 734 Ng, N. L., Canagaratna, M. R., Jimenez, J. L., Chhabra, P. S., Seinfeld, J. H., and Worsnop, D.
735 R.: Changes in organic aerosol composition with aging inferred from aerosol mass spectra,
736 *Atmos. Chem. Phys.*, 11, 6465–6474, <https://doi.org/10.5194/acp-11-6465-2011>, 2011.
- 737 Onasch, T. B., Trimborn, A., Fortner, E. C., Jayne, J. T., Kok, G. L., Williams, L. R., Davidovits,
738 P., and Worsnop, D. R.: Soot particle aerosol mass spectrometer: Development, validation,
739 and initial application, *Aerosol Sci. Technol.*, 46, 804–817,
740 <https://doi.org/10.1080/02786826.2012.663948>, 2012.
- 741 Paatero, P.: The Multilinear Engine—A Table-Driven, Least Squares Program for Solving
742 Multilinear Problems, Including the n-Way Parallel Factor Analysis Model, *J. Comput.*
743 *Graph. Stat.*, 8, 854–888, <https://doi.org/10.1080/10618600.1999.10474853>, 1999.
- 744 Sullivan, A. P., Hodas, N., Turpin, B. J., Skog, K., Keutsch, F. N., Gilardoni, S., Paglione, M.,
745 Rinaldi, M., Decesari, S., Cristina Facchini, M., Poulain, L., Herrmann, H., Wiedensohler,
746 A., Nemitz, E., Twigg, M., and Collett, J. L.: Evidence for ambient dark aqueous SOA
747 formation in the Po Valley, Italy, *Atmos. Chem. Phys.*, 16, 8095–8108,
748 <https://doi.org/10.5194/acp-16-8095-2016>, 2016.
- 749 Su, J., Zhao, P., Ge, S., and Ding, J.: Aerosol liquid water content of PM_{2.5} and its influencing
750 factors in Beijing, China, *Sci. Total Environ.*, 839, 156342,
751 <https://doi.org/10.1016/j.scitotenv.2022.156342>, 2022.
- 752 Sun, Y., Chen, C., Zhang, Y., Xu, W., Zhou, L., Cheng, X., Zheng, H., Ji, D., Li, J., Tang, X.,
753 Fu, P., and Wang, Z.: Rapid formation and evolution of an extreme haze episode in Northern
754 China during winter 2015, 1–9, <https://doi.org/10.1038/srep27151>, 2016.
- 755 Sun, Y., Xu, W., Zhang, Q., Jiang, Q., Canonaco, F., Prévôt, A. S. H., Fu, P., Li, J., Jayne, J.,
756 Worsnop, D. R., and Wang, Z.: Source apportionment of organic aerosol from 2-year highly
757 time-resolved measurements by an aerosol chemical speciation monitor in Beijing, China,
758 *Atmos. Chem. Phys.*, 18, 8469–8489, <https://doi.org/10.5194/acp-18-8469-2018>, 2018a.

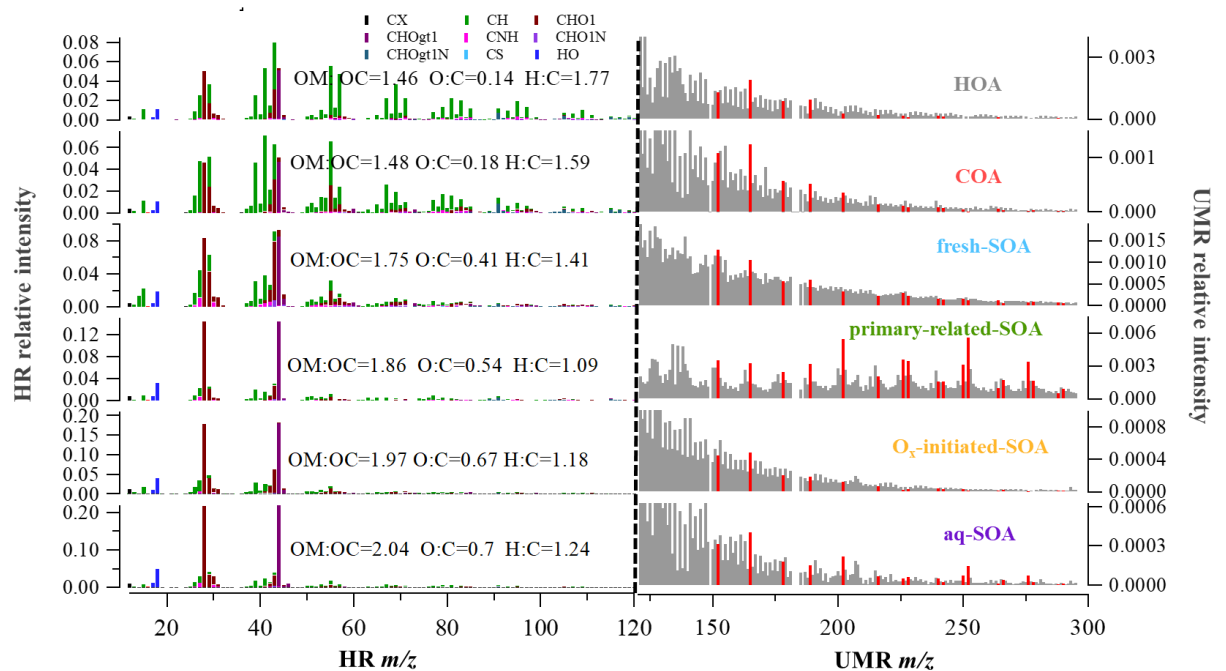
- 759 Sun, Y., Xu, W., Zhang, Q., Jiang, Q., Canonaco, F., and Prévôt, A. S. H.: Source
760 apportionment of organic aerosol from two-year highly time- resolved measurements by an
761 aerosol chemical speciation monitor in Beijing , China, 2018b.
- 762 Sun, Y. L., Zhang, Q., Anastasio, C., and Sun, J.: Insights into secondary organic aerosol
763 formed via aqueous-phase reactions of phenolic compounds based on high resolution mass
764 spectrometry, *Atmos. Chem. Phys.*, 10, 4809–4822, [https://doi.org/10.5194/acp-10-4809-](https://doi.org/10.5194/acp-10-4809-2010)
765 2010, 2010.
- 766 Wang, J., Ye, J., Zhang, Q., Zhao, J., Wu, Y., Li, J., Liu, D., Li, W., Zhang, Y., Wu, C., Xie,
767 C., Qin, Y., Lei, Y., Huang, X., Guo, J., Liu, P., Fu, P., Li, Y., Lee, H. C., Choi, H., Zhang,
768 J., Liao, H., Chen, M., Sun, Y., Ge, X., Martin, S. T., and Jacob, D. J.: Aqueous production
769 of secondary organic aerosol from fossil-fuel emissions in winter Beijing haze, *Proc. Natl.*
770 *Acad. Sci. U. S. A.*, 118, 1–6, <https://doi.org/10.1073/pnas.2022179118>, 2021.
- 771 Wang, S., Newland, M. J., Deng, W., Rickard, A. R., Hamilton, J. F., Muñoz, A., Ródenas, M.,
772 Vázquez, M. M., Wang, L., and Wang, X.: Aromatic Photo-oxidation, A New Source of
773 Atmospheric Acidity, *Environ. Sci. Technol.*, 54, 7798–7806,
774 <https://doi.org/10.1021/acs.est.0c00526>, 2020.
- 775 Xu, S., Liu, W., and Tao, S.: Emission of Polycyclic Aromatic Hydrocarbons in China,
776 *Biophys. Process. Anthropog. Org. Compd. Environ. Syst.*, 40, 267–281,
777 <https://doi.org/10.1002/9780470944479.ch11>, 2006.
- 778 Xu, W., Han, T., Du, W., Wang, Q., Chen, C., Zhao, J., Li, J., Fu, P., Wang, Z., Worsnop, D.
779 R., and Sun, Y.: Effects of Aqueous-phase and Photochemical Processing on Secondary
780 Organic Aerosol Formation and Evolution in Beijing , China,
781 <https://doi.org/10.1021/acs.est.6b04498>, 2017.
- 782 Xu, W., Sun, Y., Wang, Q., Zhao, J., Wang, J., Ge, X., Xie, C., Zhou, W., Du, W., Li, J., Fu,
783 P., Wang, Z., Worsnop, D. R., and Coe, H.: Changes in Aerosol Chemistry From 2014 to
784 2016 in Winter in Beijing: Insights From High-Resolution Aerosol Mass Spectrometry, *J.*
785 *Geophys. Res. Atmos.*, 124, 1132–1147, <https://doi.org/10.1029/2018JD029245>, 2019.
- 786 Ye, C., Liu, P., Ma, Z., Xue, C., Zhang, C., Zhang, Y., Liu, J., Liu, C., Sun, X., and Mu, Y.:
787 High H₂O₂ Concentrations Observed during Haze Periods during the Winter in Beijing:
788 Importance of H₂O₂ Oxidation in Sulfate Formation, *Environ. Sci. Technol. Lett.*, 5, 757–
789 763, <https://doi.org/10.1021/acs.estlett.8b00579>, 2018.
- 790 Zhang, Q., Jimenez, J. L., Canagaratna, M. R., Ulbrich, I. M., Ng, N. L., Worsnop, D. R., and
791 Sun, Y.: Understanding atmospheric organic aerosols via factor analysis of aerosol mass
792 spectrometry: A review, <https://doi.org/10.1007/s00216-011-5355-y>, 2011.
- 793 Zhao, J., Qiu, Y., Zhou, W., Xu, W., Wang, J., Zhang, Y., Li, L., Xie, C., Wang, Q., Du, W.,
794 Worsnop, D. R., Canagaratna, M. R., Zhou, L., Ge, X., Fu, P., Li, J., Wang, Z., Donahue, N.
795 M., and Sun, Y.: Organic Aerosol Processing During Winter Severe Haze Episodes in
796 Beijing, *J. Geophys. Res. Atmos.*, 124, 10248–10263,
797 <https://doi.org/10.1029/2019JD030832>, 2019.

798

799

800

801

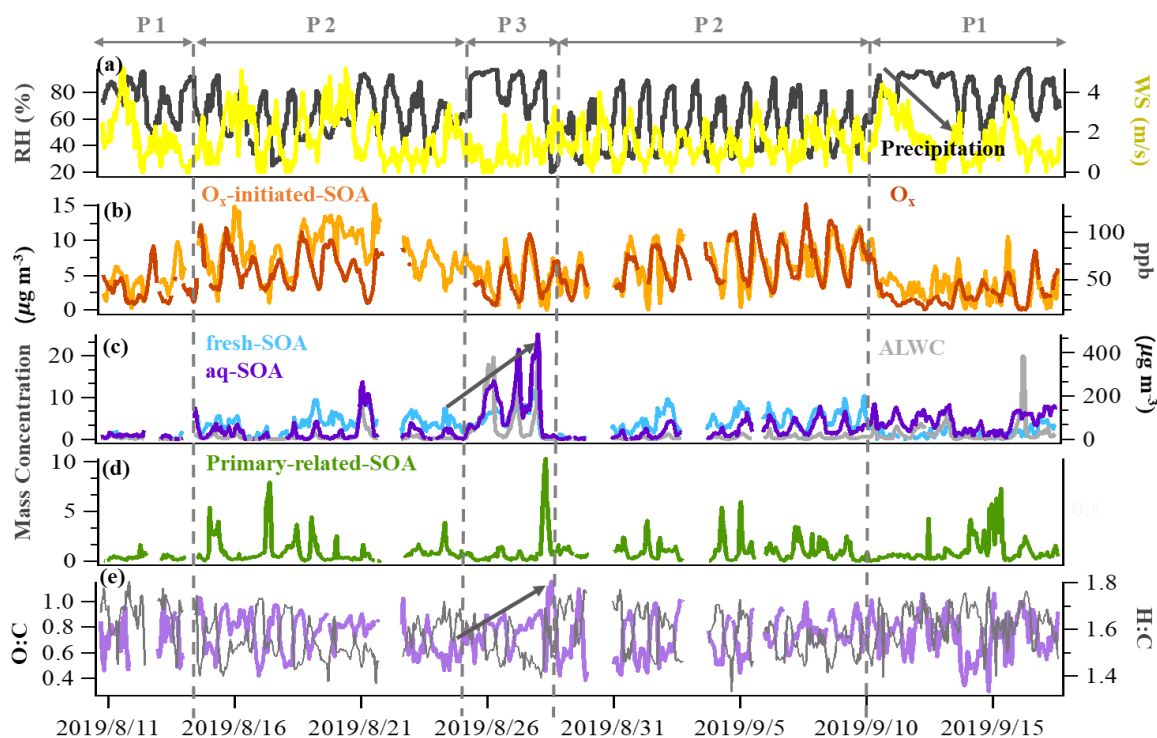
802 **Figures**

803

804 **Fig. 1** HR and UMR mass spectra of OA factors: (a) HOA; (b) COA; (c) fresh-SOA; (d)
 805 primary-related-SOA; (e) ~~phochem-SOA~~ O_x -initiated-SOA; (f) aq-SOA. Mass spectra signals
 806 less than 120 amu are colored by nine ion categories, signals equal to or greater than 120 amu
 807 are in unit mass resolution, and polycyclic aromatic hydrocarbons (PAHs) signals are in red on
 808 the right panels.

809

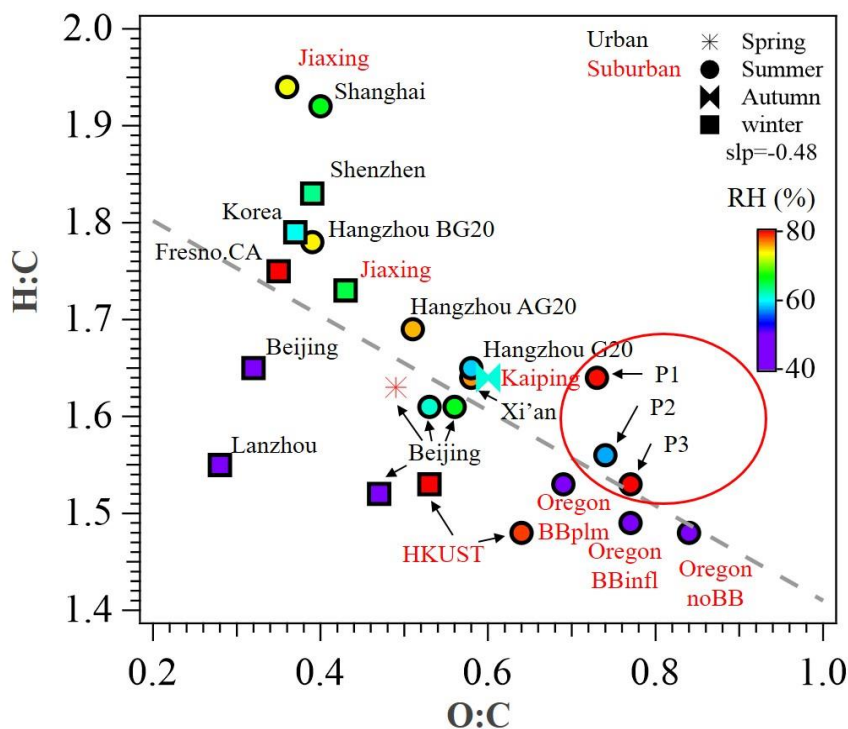
810



811

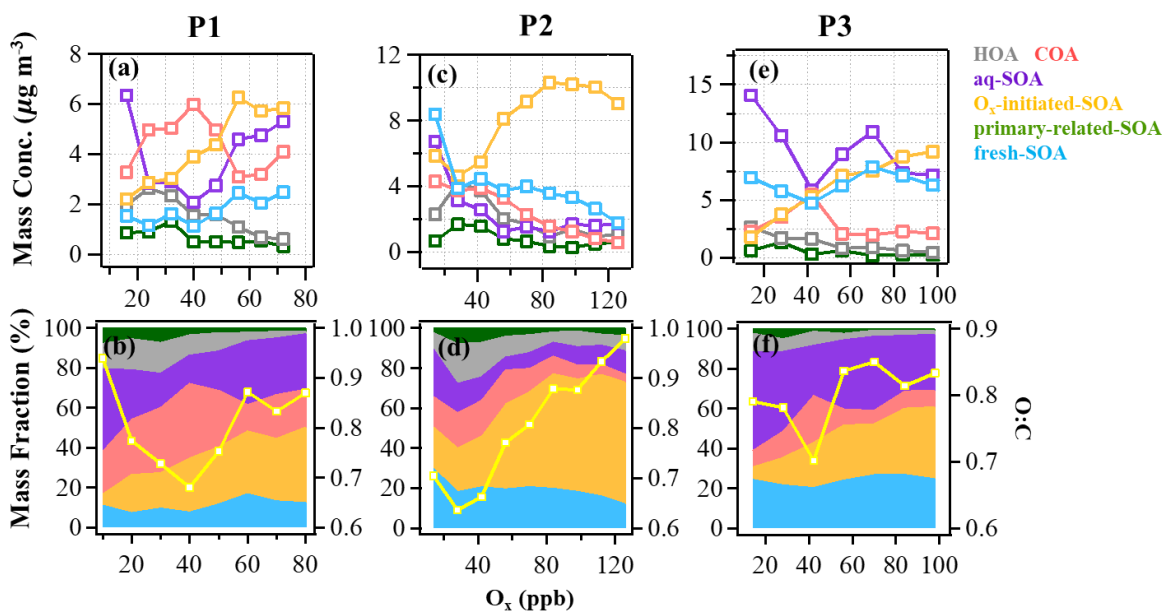
812 **Fig. 2** Time series of (a) relative humidity (RH) and wind speed (WS), (b) O_x and ~~photochem-~~
 813 ~~SOA~~O_x-initiated-SOA, (c) fresh-SOA, aq-SOA and ALWC, (d) primary-related-SOA, (e) the
 814 O:C ratio and H:C ratio. The time series were categorized to be three typical periods based on
 815 total SOA mass concentrations and meteorology conditions: reference period (P1), high O_x
 816 period (P2) and high RH period (P3).

817



818

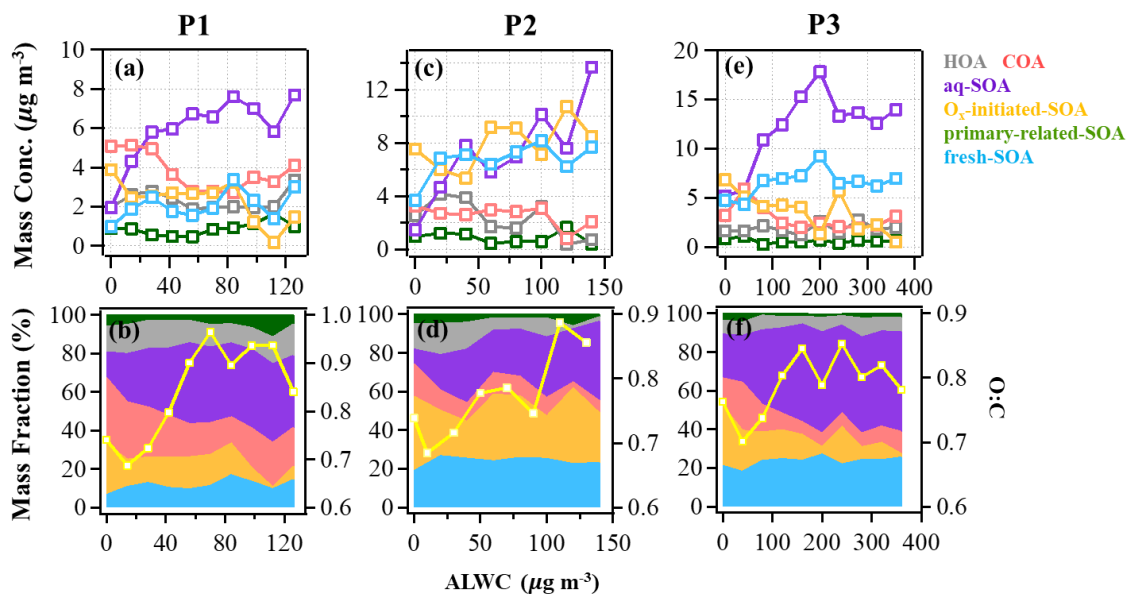
819 **Fig.3** Van Krevelen plot for OA of urban and suburban sites in China and other nations. Data
 820 points are colored by RH (%). P1, P2 and P3 in red circles represents the different periods in
 821 this study. All the data and related references can be found in Table S3.



822

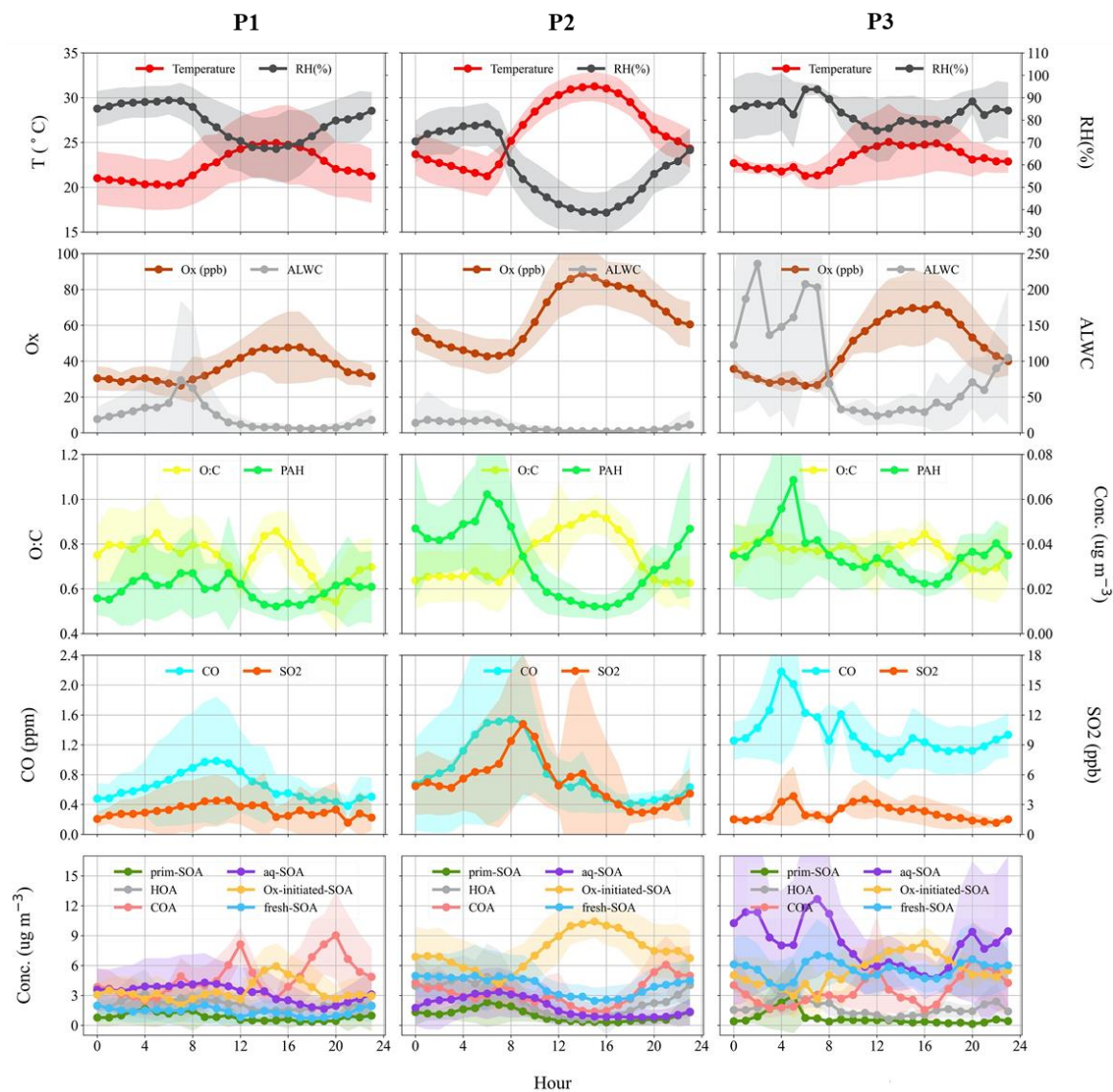
823 **Fig. 4** The mass concentration and contribution of OA factors as functions of O_x in reference
 824 period (P1: a & b), high O_x period (P2: c & d) and high RH period (P3: e & f) during this

825 campaign. The yellow curves represent the O:C ratio vs. O_x . The data were binned according
 826 to O_x concentration (10 ppb increment in P1, 14 ppb increment in P2 and P3-



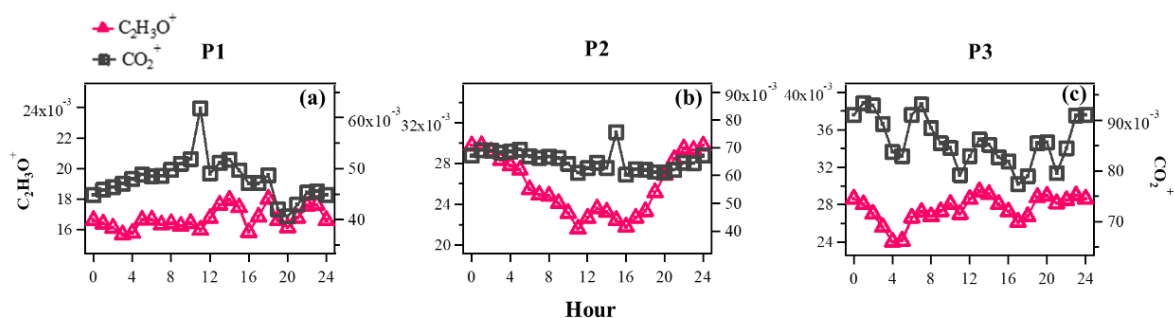
827

828 **Fig. 5** The mass concentration and contribution of OA factors as functions of ALWC in
 829 reference period (P1: a & b), high O_x period (P2: c & d) and high RH period (P3: e & f) during
 830 this campaign. The yellow curves represent the O:C ratio v.s. ALWC. The data were binned
 831 according to the ALWC concentration (14 $\mu\text{g m}^{-3}$, 20 $\mu\text{g m}^{-3}$ and 40 $\mu\text{g m}^{-3}$ increment in P1 and
 832 P2 and, in P3).



833

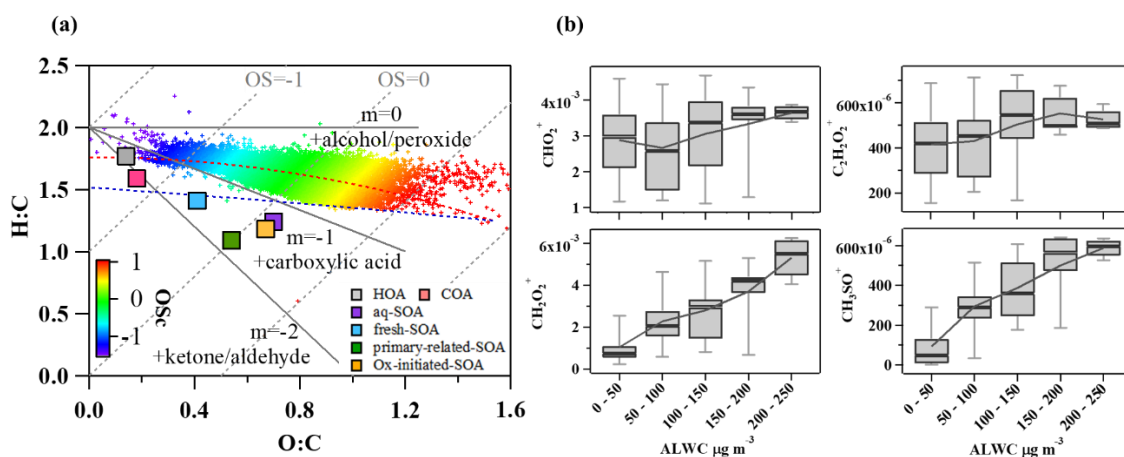
834 **Fig. 6** Diurnal patterns of meteorological parameters (T, RH), gaseous species (O_x, CO, SO₂),
 835 ALWC (liquid water content), O:C (oxygen-to-carbon elemental ratio), polycyclic aromatic
 836 hydrocarbons (PAHs) fragments and OA factors in reference period (P1), high O_x period (P2)
 837 and high RH period (P3) in this campaign.



838

839 **Fig. 7** Evolution of high-resolution organic mass spectra on changes in relative intensities (mass
 840 fraction) of oxygen-containing ions: $C_2H_3O^+$ (m/z 43) and CO_2^+ (m/z 44) in reference period
 841 (P1:a), high O_x period (P2: b) and high RH period (P3: c) in this campaign.

842



843

844 **Fig. 8** (a) Van Krevelen diagram for the O:C and H:C ratios of different OA factors (marked
 845 with squares) and bulk of OA during summer (marked with plus signs and colored by
 846 Oscarbon oxidation state (OSc)); (b) Mass fractions of ion fragments indicative of aqueous-
 847 phase processing and oxygenated functional groups (alcohols, carboxylic acids) as a function
 848 of ALWC.